RSC Advances

PAPER

View Article Online
View Journal | View Issue

Cite this: *RSC Adv.*, 2017, **7**, 40819

Phosphorus recovery as ferrous phosphate (vivianite) from wastewater produced in manufacture of thin film transistor-liquid crystal displays (TFT-LCD) by a fluidized bed crystallizer (FBC)†

Ricky Priambodo,[a] Yu-Jen Shih*[b] and Yao-Hui Huang *[ac]

In this investigation, fluidized bed crystallization (FBC) is utilized to treat phosphorus wastewater that is produced by the manufacture of thin film transistor-liquid crystal displays (TFT-LCD). TFT-LCD wastewater contains 500 ± 10 ppm phosphorus. The pH and molar ratio of Fe/P for removing phosphorus was initially examined by performing a jar-test. The parameters of the FBC – effluent pH_e, Fe/P ratio and the upflow velocity (m h^{-1}) – were tested to recover phosphorus from wastewater as ferrous phosphate pellets, characterized using an X-ray diffractometer (XRD) and scanning electron microscopy (SEM), and silica sand was used as the seed material. The experimental results revealed that the control of effluent pH_e was an essential parameter in maximizing the phosphorous removal (PR%) and crystallization ratio (CR%). At pH_e 5–6, the supersaturation of phosphate precipitation by conditioning the molar ratio of Fe/P to 1.5 and the upflow rate was adjusted within the range of 30.56–68.76 m h^{-1} in the metastable zone at a cross-section loading of 0.72 kg per P per h per m^2, leading to a phosphorus removal (PR) of 95% and a crystallization ratio (CR) of 63%. Under optimal hydraulic conditions, the treatment of real wastewater in a FBC process was viable by converting the pollutant into crystals with a high-purity phase of vivianite ($Fe_3(PO_4)_2 \cdot 8H_2O$).

Received 6th June 2017
Accepted 15th August 2017

DOI: 10.1039/c7ra06308c

rsc.li/rsc-advances

1. Introduction

Phosphorus is a critical element in agriculture and industry. It is a key nutrient for biological organisms. Eutrophication may be caused by the oversupply of phosphorus, which results in overgrowth of plants and algae in rivers and lakes.[1,2] Phosphorus is a finite resource,[3] which will be depleted over the next 100 years on account of human activities. Therefore, an effective technique for recovering phosphorus from wastewater must urgently be developed. Wastewater that contains phosphorus is typically generated by municipal, industrial and agricultural activities.[4,5] Taiwan Environmental Protection Agency imposes a standard limit of 1.4 ppm-P for wastewater.[6] In Taiwan, the manufacturing of TFT-LCD involves phosphoric acid as an etching reagent and generates large quantities of wastewater that contains high concentrations of phosphate, which varies from hundreds to a thousand ppm-P.[7,8] Methods for reclaiming phosphorus from water include biological treatment,[9] chemical precipitation,[10] adsorption,[11] electrocoagulation,[12] ion exchange,[13] and crystallization.[14] Biological methods can be used over the long-term for wastewater with a low concentration of phosphate. Chemical precipitation has been proved to be more efficient than biology.[15] The reagents that have been used to remove phosphate are Mg^{2+}/NH^{4+}, Ca^{2+}, Al^{3+}, which recover struvite,[16,17] brushite,[18] hydroxyapatite,[19] and berlinite.[20,21] However, chemical precipitation and coagulation normally generate sludge that contains a high level of moisture. The disposal of sludge, including filtration, sedimentation and dewatering, is responsible for a considerable ratio to the budget of wastewater treatment.[22]

Since the 1990s, fluidized-bed crystallization (FBC) has been extensively used to overcome the shortcomings of chemical precipitation during the management of wastewater.[23,24] Proper crystallization of the target compound in an FBC reactor depends on the hydraulic conditions, which must allow particles sufficiently to collide with each other and to repel most of the water among the fine nuclei.[14] The aquatic condition that controls supersaturation when a solute exceeds its solubility limit determines the efficiency of crystal growth. Typically, the

[a]*Department of Chemical Engineering, National Cheng Kung University, Tainan 701, Taiwan. E-mail: yhhuang@mail.ncku.edu.tw; Fax: +886-6-234-4496; Tel: +886-6-275-7575-62636*

[b]*Institute of Environmental Engineering, National Sun Yat-sen University, Kaohsiung 804, Taiwan. E-mail: mcdyessjin@gmail.com; Tel: +886-973-155271*

[c]*Sustainable Environment Research Center, National Cheng Kung University, Tainan 701, Taiwan*

† Electronic supplementary information (ESI) available. See DOI: 10.1039/c7ra06308c

phosphate removal from wastewater plants is mostly recovered as agricultural uses, like fertilizer (struvite, hydroxylapatite). Considering that vivianite is an important source in the manufacture of lithium iron phosphate ($LiFePO_4$), which has been extensively applied to fabricate the Li-ion secondary batteries,[25,26] the reclamation of phosphate in the form of the mineral vivianite is a potential alternative to chemical precipitation as a sustainable method for the reuse of phosphorus. Very few studies involve the use of ferrous salt as a precipitant and the crystallization of vivianite to reduce the phosphorus content in wastewater. In this investigation, wastewater from the manufacture of TFT-LCD was treated in an FBC reactor, successfully recovering crystals of ferrous phosphates (vivianite). Experimental parameters, including pH effluent, Fe/P ratio and the upflow velocity (m h^{-1}), which were critical in estimating the suitable supersaturation of a FBC process,[27,28] were evaluated based on the criteria of phosphorus removal (PR%) and crystallization ratio (CR%) (or conversion rate, % (ref. 23 and 24)).

2. Materials and methods

2.1 Chemicals

All reagents were of analytical grade, and used without further purification. The real wastewater used in the present work was obtained from a TFT-LCD company in Taiwan. The characteristics of the wastewater is as listed in Table 1. Ferrous sulfate heptahydrate ($FeSO_4 \cdot 8H_2O$, Sigma-Aldrich Co. LLC., USA) was used as the iron source. The solution pH was adjusted by sodium hydroxide (NaOH, Merck KGaA, Germany) and nitric acid (HNO_3, Sigma-Aldrich, USA). The waters for all chemicals were doubly deionized using a laboratory-grade RO-ultrapure water system (resistance > 18.3 MΩ).

2.2 Experimental procedure

The jar test was conducted in 1000 mL glass beaker. The precipitation was started by adding a specific amount of ferrous sulfate to the wastewater of which pH has been adjusted, and the mixture was stirred by 100 rpm for 5 min, and then by 30 rpm for 20 min. To minimize the oxidation of iron, the jars were covered with plastic caps and the solution was purged with the nitrogen gas during the precipitation reaction. The sample was filtrated using 0.22 μm filter after 24 hours, and the filtrate was directly digested with 1 mL HNO_3 (70%) (to stop the precipitation). The fluidized bed reactor is a cylindrical column made of Pyrex glass with a capacity of 500 mL (including main body of reactor and pipelines) as revealed in Fig. 1. Two parts of fluidized-bed reactor are connected with a sudden enlarged joint constitute the main body of reactor. The lower part is 2 cm in inner diameter and 80 cm in height. The upper part is 4 cm in inner diameter and 15 cm in height. Such sudden expansion can reduce the hydraulic loading and prevent too much fines from being drained out. Two peristaltic pumps are used for pumping the inflows of ferrous sulfate and wastewater and one peristaltic pump is used to control the reflux flow rate. (The photograph of FBC reactor setup for the treatment of phosphorus wastewater is as depicted in Fig. S2 in the ESI.†) A static bed of silica sand ($D_{50} \sim 0.2$ mm, granular SiO_2, quartz phase) was then made at a level of around 30 cm. Sampling and pH monitoring were conducted from the effluent at the upper column. Important parameters and their corresponding nomenclature are summarized in Table 2.

Table 1 Characteristics of wastewater

	Compositions
pH	7.3 ± 0.3
PO_4^{3-}–P	500 ± 10 ppm
K	42.8 ± 2 ppm
Na	1240 ± 20 ppm
Cl	120 ± 5 ppm
Al	5 ± 0.5 ppm
TOC	20 ± 0.2 ppm

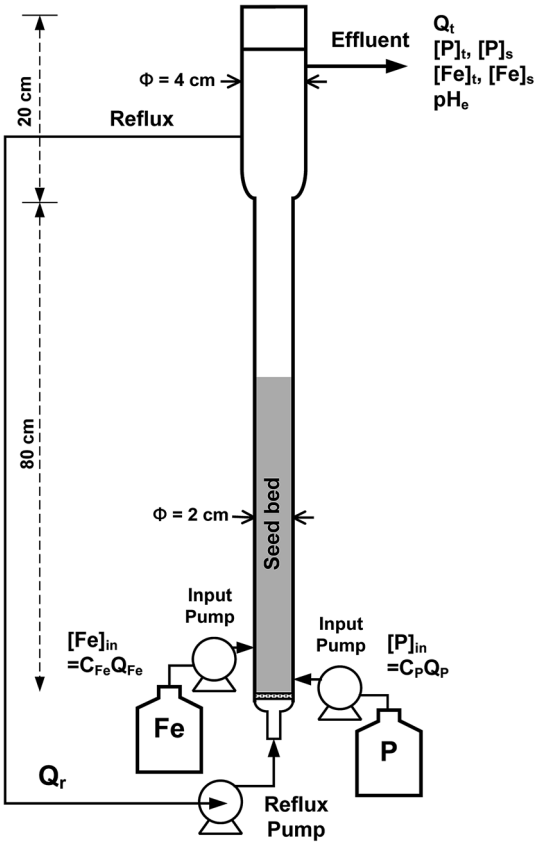

Fig. 1 Configuration of the fluidized-bed crystallization.

Experiments of phosphorus removal by FBC process were initiated by introducing the feeds of iron solution and wastewater at given flow rates, the ratio of reflux (Q_r) and influx flows ($Q_t = Q_P + Q_{Fe}$) under room temperature (25 ± 1 °C). (To minimize the oxidation of iron, the solution in Fe(II) tank was purged with the nitrogen gas before it was introduced into the reactor.) Hydraulic retention time (HRT) under a specific bed height was adjusted through the control of the influx flow rate

Table 2 Experimental parameters for ferrous phosphate crystallization in FBC

Symbol	Definition	Unit	Remarks
Q_{Fe}, Q_P	Influx of Fe and P ions	mL min^{-1}	
Q_t	Total influx flow rate	mL min^{-1}	$=Q_{Fe}+Q_P$
Q_r	Reflux flow rate	mL min^{-1}	
C_{Fe}, C_P	Concentrations of Fe and P ions in feed tank	M	
$[Fe]_t$, $[Fe]_s$	Total and soluble Fe ions in effluent	M	
$[P]_t$, $[P]_s$	Total and soluble P in effluent	M	
$[Fe]_{in}/[P]_{in}$	Inlet molar ratio		$=C_{Fe}Q_{Fe}/C_PQ_P$
A_{low}	Internal cross-section area of reaction region	cm^2	
A_{up}	Internal cross-section area of effluent region	cm^2	
U_{out}	Effluent velocity	m h^{-1}	$=Q_t/A_{up}$
U	Upflow velocity (hydraulic loading)	m h^{-1}	$=(Q_t+Q_r)/A_{low}$
L	Cross-section loading	kg m^{-2} h^{-1}	$=C_PQ_P/A_{low}$
V_T	Total volume of reaction solution in reactor	mL	
HRT	Hydraulic retention time	min	$=V_T/Q_t$
pH_e	Effluent pH		

(15–75 mL min^{-1}, for both of phosphorus and ferrous, while the corresponding reflux flows were 120–0 mL min^{-1}). The silica sand as the seed was filled into reactor to reach a static bed height of 30 cm. The stock solutions of phosphorus wastewater and iron with given concentrations were then introduced into FBC. The pH of wastewater was controlled using NaOH and HNO_3, whereas the pH of ferrous sulfate was maintained at the level of pH 2 to prevent the oxidation of ferrous ions. A typical run for pH and aquatic measurements lasted at least 9 HRT after changing the parameters of whole system, such as pH, influx concentration. (The FBC system for creating vivianite crystals typically reached an equilibrium in 5–7 HRT as shown in Fig. S3,† so the experimental results obtained were recorded at 9 HRT.) For every sampling, 10 mL solution was withdrawn at effluent twice: one was filtered with a 0.22 μm filter and the other was not. Both liquids with and without filtration were then acid digested with 1 mL HNO_3 (70%). Phosphate and iron ions in digests were $[P]_t$ and $[Fe]_t$, and in filtrates were $[P]_s$ and $[Fe]_s$. Two calculations were therefore used to verify the efficacy of FBC process, phosphorous removal (PR%) and crystallization ratio (CR%).[29–31]

$$PR\% = \left(1 - \frac{[P]_s \times Q_t}{C_P \times Q_P}\right) \times 100 \quad (1)$$

$$CR\% = \left(1 - \frac{[P]_t \times Q_t}{C_P \times Q_P}\right) \times 100 \quad (2)$$

The influent mass of P was eventually converted into three forms, which were soluble P, fine precipitates (unsettled flocs) and large crystals that were fluidized in the reactor. PR% is used to evaluate the efficiency of FBC in reducing phosphorous from aqueous phase, while CR% refers to the recoverability of the ferrous phosphate as coarse pellets. At the end of the experiment the pellets were removed from the bottom of the bed and air-dried for further characterization.

The reaction between ferrous and phosphorus can be seen in eqn (3)

$$3FeSO_4\cdot 7H_2O + 2PO_4^{3-} \rightarrow Fe_3(PO_4)_2\cdot 8H_2O + 3SO_4^{2-} + 13H_2O \quad (3)$$

2.3 Analytical methods and characterization

Concentrations of P, Fe and other elements (see Table S2†) in samplings were determined by an inductively coupled plasma-optical emission spectrometer (ICP-OES, ULTIMA 2000, HORIBA Ltd., Japan). A scanning electron microscopy (SEM, JSM-6700F, JEOL Ltd., Japan) was used to observe the micro-morphology of FBC products. While the surface composition was analyzed by the attached energy dispersive spectrometer (EDS, LINKS AN10000/85S). X-ray diffraction (XRD, DX III, Rigaku Co., Japan) patterns determined the crystallographic structure was operated with Cu Kα radiation source (λ = 1.5406 Å) and a scanning rate of 10° min^{-1} in the incidence angle range of 10–90° (2θ). Total organic carbon (TOC) was measured using a TOC analyzer (Sievers innovox, GE power, U.S.A).

3. Results and discussion

3.1 Jar-test of ferrous phosphate precipitation

Jar-tests were performed to evaluate the effect of pH on the removal of phosphorus by the precipitation of $Fe_3(PO_4)_2\cdot 8H_2O$. The pH range was 2.0–11.0 and the Fe/P ratio was 1.5. Fig. 2a demonstrates that the phosphorus removal increased with pH; in particular, an increase in pH from 2.0 to 6 increased the removal of phosphorus from 20% to 96.2%. The chemical precipitation was optimized at a pH of 7 to 8 (PR > 99.9%). However, PR decreased as pH increased above 8. The effect of pH on the precipitation of slightly soluble or insoluble salts was related to the solubility product. Restated, the driving force of formation of new nuclei subject to supersaturation was definitely influenced by the solubility product constants (K_{sp}).[32]

$$Fe_3(PO_4)_2\cdot 8H_2O \rightarrow 3Fe^{2+} + 2PO_4^{3-} + 8H_2O,\ K_{sp} = 10^{-35.8} \quad (4)$$

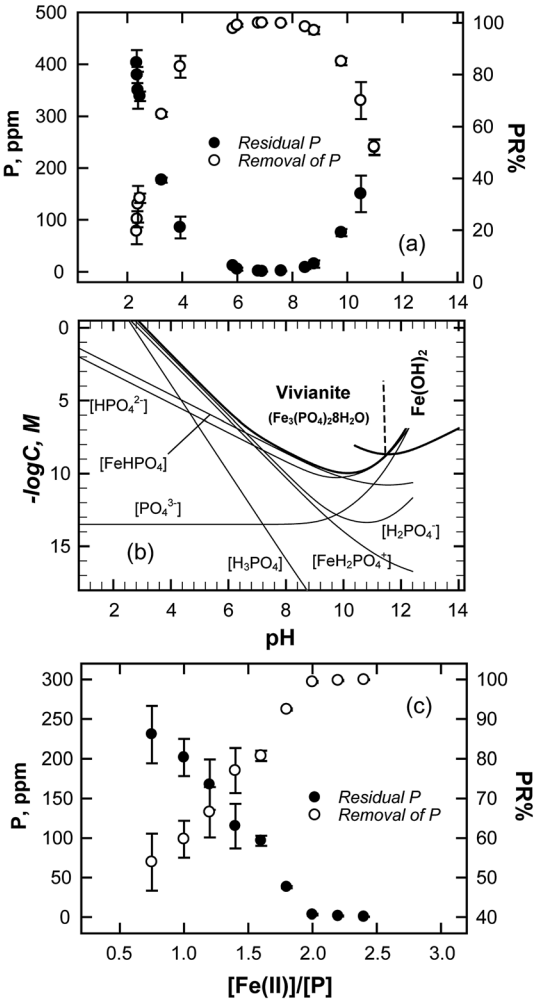

Fig. 2 (a) Effects of pH on the phosphate removal and residual P by jar-test (pH = 2–11, [Fe(II)]/[P] = 1.5, $[P]_{in}$ = 500 ppm). (b) Solubility curves of ferrous phosphate ($Fe_T = 10^{-3}$ M) and ferrous hydroxide. Effect of the molar ratio of Fe(II)/P on the phosphate removal of jar test (pH = 8, $[P]_{in}$ = 500 ppm).

The soluble ions (Fe(II) and P) and the solid phase were in equilibrium with a constant of free ionic activities product,

$$K = \{Fe^{2+}\}^3\{PO_4^{3-}\}^2 = [Fe^{2+}]^3[PO_4^{3-}]^2\gamma_{Fe}^3\gamma_{PO_4}^2 \quad (5)$$

where γ_{Fe} and γ_{PO_4} are the activity coefficients of iron and phosphate ions. The supersaturation ratio or relative saturation index (β) is therefore defined as $\beta = \ln(K/K_{sp})$. β is related to the Gibbs free energy, which determines whether the precipitation occurs spontaneously ($\Delta G = -RT \times \beta$). At equilibrium, K equals K_{sp}, so $\Delta G = 0$. In the presence of seeds that promote the nucleation in the reactor, the dissolved solute was continuously converted to the solid phase when $K > K_{sp}$ ($\Delta G < 0$, indicating spontaneous precipitation).[33,34] A mathematical model is proposed to calculate the conversion of Fe–P–H_2O at given pH and concentrations of the solute: $[PO_4^{3-}]$ is a function of total soluble phosphate concentration $[P]_s$ with a proportionality that is dominated by pH.

$$\begin{aligned}[P]_s &= [PO_4^{3-}] + [HPO_4^{2-}] + [H_2PO_4^-] + [H_3PO_4] \\ &\quad + [FeH_2PO_4^+] + [FeHPO_4] \\ &= [PO_4^{3-}]\left(1 + \frac{[H^+]}{K_{a3}} + \frac{[H^+]^2}{K_{a2}K_{a3}} + \frac{[H^+]^3}{K_{a1}K_{a2}K_{a3}}\right) \\ &\quad + [Fe^{2+}][PO_4^{3-}]\left(K_4[H^+]^2 + K_5[H^+]\right) \\ &= [PO_4^{3-}]/\alpha_P \end{aligned} \quad (6)$$

K_4 and K_5 are the formation constants of the ferrous phosphate complexes $FeH_2PO_4^+$ and $FeHPO_4$. Total soluble iron comprise Fe^{2+} and the hydrolyzed species.

$$\begin{aligned}[Fe]_s &= [Fe^{2+}] + [Fe(OH)^+] + \left[Fe(OH)_{2(aq)}\right] + [Fe(OH)_3^-] \\ &\quad + [FeH_2PO_4^+] + [FeHPO_4] \\ &= [Fe^{2+}]\left(1 + \frac{K_1}{[H^+]} + \frac{K_2}{[H^+]^2} + \frac{K_3}{[H^+]^3}\right) + [Fe^{2+}][PO_4^{3-}] \\ &\quad \times \left(K_4[H^+]^2 + K_5[H^+]\right) \\ &= [Fe^{2+}]/\alpha_{Fe} \end{aligned} \quad (7)$$

Thus, the solubility of phosphate is determined by α_{Fe} and α_P, which are functions of the background concentrations of protons, iron and phosphate species.

$$[P]_s = \left\{\frac{K_{sp}}{([Fe]_s\alpha_{Fe})^3\alpha_P^2}\right\}^{1/2} \quad (8)$$

(The ESI† provides details of the calculation and the equilibrium constants). As predicted from solubility curve in Fig. 2b, the effects of pH on PR can be explained by the precipitation of ferrous phosphate and the speciation of phosphate anions. At a pH of less than 6 $[P]_s$ increases with an increase in the solubility of $Fe_3(PO_4)_2 \cdot 8H_2O$ so PR increases with pH. The measured phosphorus concentration reaches its lowest value at pH 7–8, which differs from the minimum of the solubility curve, because of the competition of ferrous hydroxide precipitation with ferrous phosphate, which consumes a significant amount of iron. Hence, as pH increases above 8.5, PR decreases. Based on the results of the jar-test, FBC yields an effective in PR in a pH range of 7–8, with pure ferrous phosphate crystallization (by minimizing the co-precipitation of $Fe(OH)_2$).

From the chemical formula of vivianite, the stoichiometric ratio of Fe(II) to P is 1.5. In the jar-test, however, PR increases with Fe(II)/P, reaching a maximum (99.5%) at Fe(II)/P = 2, as presented in Fig. 2c, at which ratio the phosphate concentration has decreased to below 3 ppm. The optimal molar ratio of Fe(II)/P by chemical precipitation exceeded the stoichiometric value for vivianite, because the standard procedure was used in the jar-test. Since all experiments were conducted in 25 min (with fast stirring for 5 min), followed by a slow stirring for 20 min, and then left to stand for 24 h, phosphate removal may have involved the precipitation of ferric phosphate after the oxidation of Fe(II) to Fe(III). However, $FePO_4$ ($K_{sp} = 10^{-21.9}$) is

thermodynamically disfavored relative to the formation of ferric hydroxide ($K_{sp} = 10^{-38.55}$),[35] which may consume iron and compete against the formation of vivianite (the solubility curves of $Fe(OH)_3$, $FePO_4$ and vivianite are as plotted in Fig. 4S†). Since the jar-test was carried out to figure out the influence the ratio of Fe/P on the removal of phosphate, the overdose of iron that increased the supersaturation of $Fe(OH)_3$ and competed the precipitation of vivianite had to be considered. The existing of $Fe(OH)_3$ can also be evidenced by the change in the appearance of sludge collected after jar test; as indicated in Fig. S4 in the ESI,† the precipitates turn from deep blue color to dark yellow and brown as the molar ratio of Fe(II)/P is increased.

3.2 Phosphate removal by formation of vivianite crystal in an FBC reactor

The efficiency of the FBC process is fundamentally controlled by the solubility of vivianite, which affects the resulting PR and CR. Vivianite crystallization is governed by effluent pH, Fe/P ratio and upflow velocity (m h^{-1}). The difference between PR and CR is related to the presence of fines, and therefore to the quantity of phosphorus that is lost in the effluent stream.[36] In this study, the effects of pH on the crystallization of vivianite in an FBC were examined. Fig. 3a plots PR and CR as a function of pH_e. PR increases with effluent pH (from 40% to 98.91%) and approaches its maximum of around 98% at pH values of greater than 6.[37] However, the efficiency of CR increases from 27% to 60.23% as the pH of the effluent increases from 4 to 5.8, and declines as the pH rises above 6. The ferrous phosphate precipitates is basically thermodynamically determined, while the creation of vivianite crystals as large pellets that are fluidized in the reactor is affected by the degree of supersaturation (β). Fig. 3b compares the residual P (*i.e.* $[P]_s$ which is expressed as $-\log$ P with a unit of molar concentration, M) experimentally measured from FBC reactor and the theoretical P ($[P]_{s,\ theo}$) that are estimated by substituting the concentrations of soluble iron into eqn (6)–(8) as a function of effluent pH. The deviation of the residual P from the computed solubility therefore gives a value of β ($=\ln([P]_s/[P]_{s,\ theo})$). Accordingly, at low pH (<6), the increases in CR follow that of PR since β is low and averagely in a range of 1 to 1.5, and thus most of the vivianite grows heterogeneously on the coarse pellets; at high pH (>6), $[P]_s$ deviates remarkably from the solubility limit of phosphate, yielding a β increases with increasing pH. As a result, the instantaneous formation of fines is preferred and CR is low.[38] Restated, $[P]_s$ which is an equilibrium value, or precisely

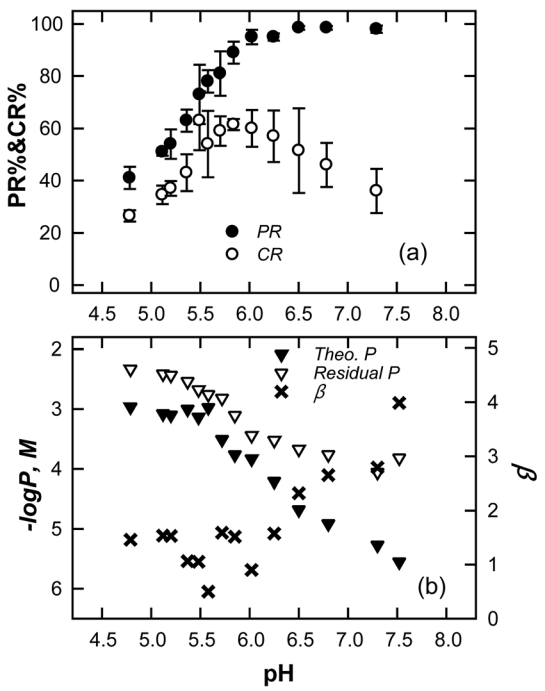

Fig. 3 (a) Effects of effluent pH ([Fe(II)]/[P] = 1.5, U = 40.11 m h^{-1}) on the crystallization ratio and phosphate removal by FBC process (Q_{Fe} = 30 mL min^{-1}, Q_P = 30 mL min^{-1}, Q_r = 150 mL min^{-1}, expanded bed height = 0.6 m; HRT = 8 min); (b) the correlation of the degree of supersaturation, the residual P and theoretical P estimated by solubility product of vivianite.

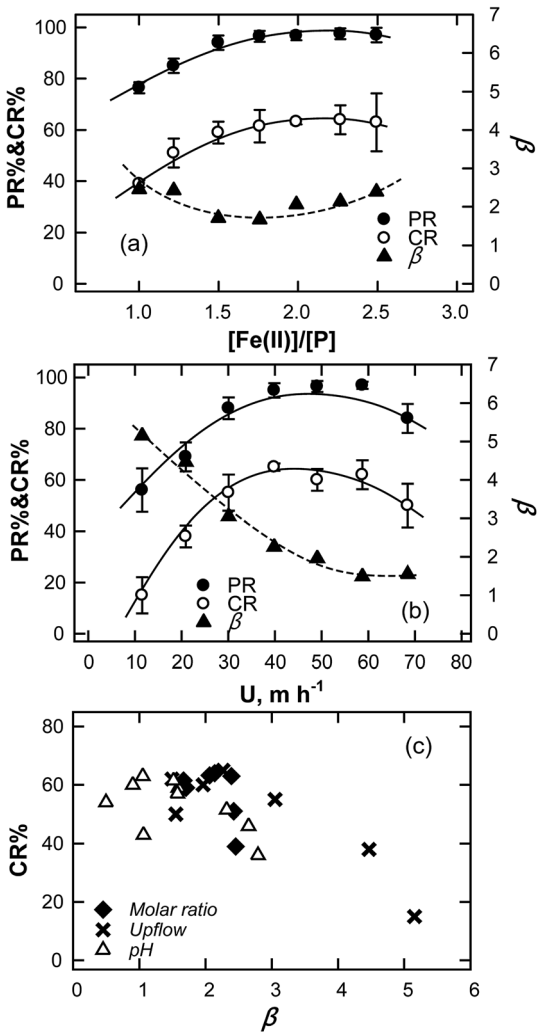

Fig. 4 Effect of (a) input molar ratio of Fe(II)/P (pH = 5.8 ± 0.2, U = 40.11 m h^{-1}) and (b) upflow velocity (pH = 5.8 ± 0.2, [Fe(II)]/[P] = 1.75) on the crystallization ratio, phosphate removal and supersaturation in FBC reactor. (c) Relationship between the degree of supersaturation and CR of vivianite under various hydraulic conditions.

a steady-state one, relative to the ideal solubility that is estimated by K_{sp} reflects the *in situ* supersaturation; therefore as it declines, supersaturation decreases, and CR increases as well. Therefore, the degree of supersaturation for vivianite crystallization is optimized at pH 5.8 where soluble P in equilibrium with phosphate solid is supposed to be in the metastable region.

To evaluate the effect of the input Fe(II)/P molar ratio in an FBC on the treatment of a solution that contains 500 ppm-P, experiments were carried out with a range of molar ratios of iron to phosphorus (1–2.5). Fig. 4a reveals that at a Fe/P molar ratio of unity, PR and CR were 76.28% and 40.84%, respectively. When the Fe/P ratio was adjusted to the stoichiometric value of vivianite (Fe/P = 1.5), PR and CR were 95.01% and 59.84%, respectively. Increasing Fe/P to 2, yielded a slightly higher PR of 97.24%. However, CR increased with Fe/P and approached to its maximum at an Fe/P of greater than 1.75, implying that the amount of input ferrous ions associated with phosphate, should exceed that determined from the stoichiometric ratio of the final precipitate, driving the precipitation (to maintain proper supersaturation).[39] The hydrodynamic conditions in an FBC affect the morphology and size of the obtained crystals. In this study, most of the precipitation reaction occurred at the bottom of the reactor and the fines were immobilized on the fluidized seeds. The solution was mixed by reflux using a peristaltic pump with a controlled speed. The upflow velocity of the fluidized bed system (U), hydraulic loading (11.46–68.76 m h^{-1}), that was used for FBC was adjusted by varying the reflux flow rate (Q_R) while the influx flow rate (Q_i) and cross-section loading were maintained at 60 mL min^{-1} ($Q_{Fe} = Q_P = 30$ mL min^{-1}) and 0.72 kg per P per h per m^2, respectively. Since the reflux flow that was used to control the total hydraulic loading (diluted the input chemical concentration), the degree of supersaturation at the bottom region was variable. As presented in Fig. 4b, the highest PR (~95%) and CR (~63%) were attained by conditioning U in the range of 30.56–68.76 m h^{-1}. The low mixing energy in the reactor that was associated with a low U (30.56 m h^{-1}) resulted in either small bed expansion or a small effective surface area. At high U, by contrast, the large bed expansion increased the length of the path of mass transport and so reduced the reactivity of the fluidized media in the reactor, yielding a low CR. In Fig. 4a and b, the degree of supersaturations were estimated by $\beta = \ln([P]_s/[P]_{s,\ theo})$ where the theoretical phosphate levels ($[P]_{s,\ theo}$) were computed from the solubility product of viviante and the measures of effluent iron concentrations (as listed in Table S1†) and pH (eqn (8)). The results reveal a moderate correlation between the crystallization of vivianite and β in the FBC reactor. Fig. 4c plotted the CR values against the β that were yielded under various operative conditions, including the upflow velocity, molar ratio of Fe(II)/P and pH. It is worth noting that the highest CR is attained at a β of around 2. Below this value, the low PR was subject to the low CR at which the β could not easily drive all the soluble phosphate ions to precipitate. When β increased beyond 3 that resulted from decreasing the upflow velocity, CR declined drastically. Accordingly, a low hydraulic loading is equivalent to a low dilution factor at the bottom of FBC reactor, and thus

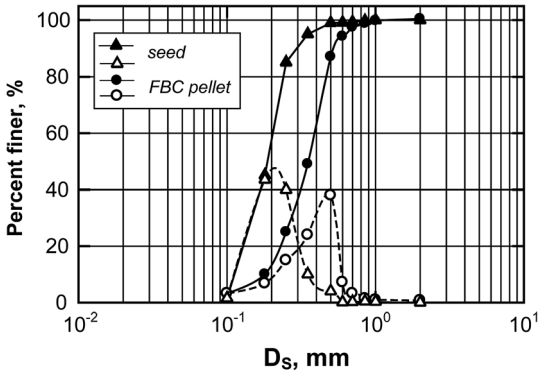

Fig. 5 Distributive and cumulative particle sizes of seed and FBC pellets (after 200 h operation of FBC under conditions of pH = 5.8 ± 0.2, [Fe(II)]/[P] = 1.75, U = 40.11 m h^{-1}).

the precipitates of vivianite is not easy to grow in such a labile zone.

In FBC process, the fluidization occurs in an upflow stream that the drag force on pellets can be comparable to the gravitational force on them. Based on Ergun model, a minimum fluidization velocity (U_{mf}) is used to define an upflow required to initiate the bed being fluidized (for low Reynolds number, Re < 10, less turbulent).[40]

$$U_{mf} = \frac{\Phi^2 D^2 {\varepsilon_{mf}}^3 (\rho_s - \rho_w) G}{150\eta(1 - \varepsilon_{mf})} \quad (9)$$

Φ and D denote the sphericity and mean diameter (cm) of the pellets; ρ_s and ρ_w are specific gravities of particles and water, respectively (g cm^{-3}); G equals to 980 cm s^{-2}, and η is the viscosity of water, 0.00894 g cm^{-1} (25 °C). The void fraction of the bed at minimum fluidization, ε_{mf}, is 0.48. The void fraction was measure using eqn (10).

$$\varepsilon = 1 - \frac{\rho_{bed}}{\rho_{solid}} \quad (10)$$

ρ_{bed} and ρ_{solid} are specific gravities of bed and crystal, Fig. 5 depicts the particle size distributions (PSD) of FBC pellets before and after 200 h of operation; the seed sample had a mass-median-diameter (D_{50}) of 200 μm, and the size of the pellets was increased to *ca.* 0.45 mm (100 g of samples were taken for each analysis of PSD, determined by sieve analysis with mesh size in a range from 0.125 mm to 0.2 mm). It was supposed that phosphate would be recovered as vivianite heterogeneously crystallized on these particles that were composed of a sand core and a ferrous phosphate shell, leading to a ρ_s of 2.59 g cm^{-3}. Consequently, U_{mf} of FBC is 21.2 m h^{-1}, which means the reactor should be operated at an upflow 1.5 to 3 times greater than its minimum fluidization velocity to optimize the crystallization ratio (or vivianite crystal conversion) from a FBC process.

3.3 Characterization of FBC product

Fig. 6 displays the SEM micromorphology of the seed and FBC products. The seed particles had rough surfaces and irregular

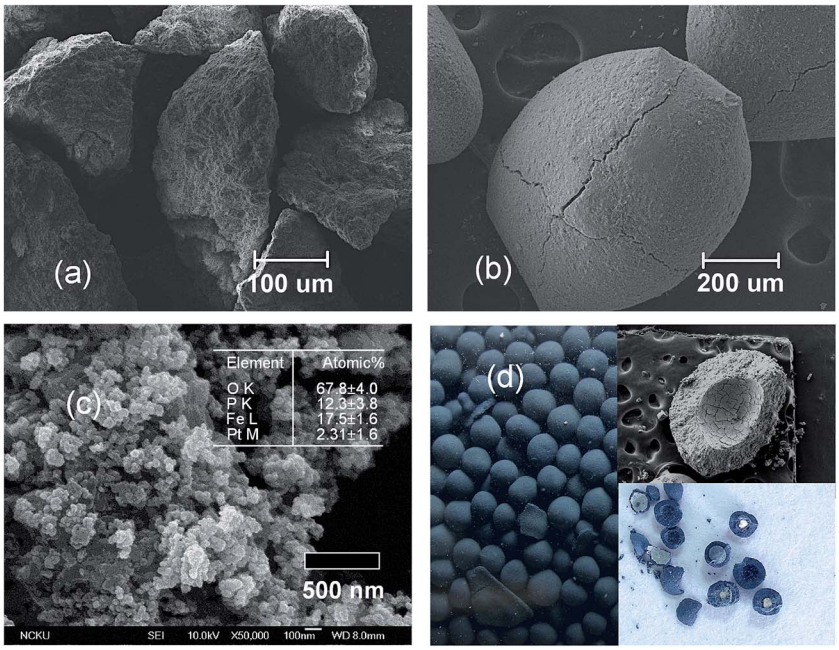

Fig. 6 SEM observation of (a) silica sand, and crystal pellets obtained from FBC process with magnification of (b) ×100, (c) ×30 000. (d) Vivianite particles recovered from FBC reactor.

shapes (Fig. 6a). After 200 h of FBC operation, the surfaces of the vivianite crystal were seen to be smoother than those of the seeds (Fig. 6b), and under high magnification the crystal comprised small fines, which were densely packed (Fig. 6c). The FBC process utilized silica sand as a fluidized medium to collect the products *via* particle collision. Owing to the sudden expansion at the upper part of the FBC reactor, the upflow velocity falls greatly and colloidal fines collide with each other, becoming larger aggregates. Such fines were created either homogeneously in bulk solution or heterogeneously on the fluidized media, adhered to the surface of the particles. Sufficiently big particles would settle down to the bottom region of the reactor and fluidize by the upstream. The sands used in FBC exerts physical force on the particle collision, promoting the layering and attrition of the coated vivianite. Fig. 6d indicates a photograph of deep blue vivianite pellets that were obtained in an FBC process (Fig. S5† exhibits the pellets from FBC process have same color with that of sludge from jar test). The dissolved oxygen may influence the oxidation of Fe(II) during operation of FBC. Although the liquid surface on the top of reactor is small (4 cm), the effect of oxidation on the crystallization rate to produce vivianite has to be considered. However, the deep blue color of the vivianite pellets suggestes that the oxidation because of being exposed to atmosphere is negligible. (Some researches also claimed that a pure vivianite was colorless, while the blue color refers to some Fe(II) has been partially oxidized as a metavivianite.[41])

The XRD results in Fig. 7 indicate that the ferrous phosphate that was recovered from both chemical precipitation (jar-test) and the FBC reactor (at pH = 5.8 ± 0.2) was pure vivianite ($Fe_3(PO_4)_2 \cdot 8H_2O$, #83-2453). During precipitation, the oxidation of ferrous ions might have competed with the consumption of iron for ferrous phosphate formation, producing ferric hydroxide. Therefore, PR was maximized (99.5%) at Fe(II)/P = 2, whereas the amount of iron sludge that was poorly crystallized increased with the ratio of ferrous to phosphate ions (from Fe(II)/P = 1 to 2.4) and the amount of mineral vivianite decreased.[42] In contrast, the weak background noise in the XRD pattern of the FBC product suggests that the ferrous phosphate pellets exhibited greater crystallinity than when the ferrous phosphate in the sludge. The signal from quartz was obtained as a result of the addition of seed material. The crystalline sizes (D_S) of vivianite that were obtained in the jar-test and the FBC process are 30.9 and 40.8 nm, respectively, determined using the Scherrer method ($D_S = 0.89\lambda/B \cos\theta$, $\lambda = 0.1546$ nm, B = full width at half maximum of peak of $(\bar{1}10)$ plane at 2θ of approximately 13.2°). Therefore, the primary grains of vivianite that

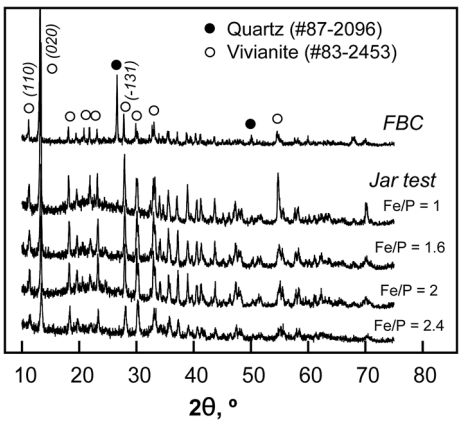

Fig. 7 X-ray powder diffraction patterns (XRD) of the crystallization products collected from the FBHC processes at pH_e 5.8 ± 0.2.

Table 3 Elemental analysis and composition of crystal pellets of $Fe_3(PO)_4 \cdot 8H_2O$

Elemental	wt%
Fe	26.9 ± 0.07
P	10.2 ± 0.02
Al	0.88 ± 0.002
Na	4.02 ± 0.04
Si	4.66 ± 0.15
Composition	
$Fe_3(PO_4)_2 \cdot 8H_2O$	81.8 ± 0.21
Quartz	9.98 ± 0.67
Water content	3.36 ± 0.7

grew during fluidized-bed treatment were slightly larger than that obtained by chemical precipitation. Nevertheless, most of the pellets with sub-millimeter or millimeter-sizes were formed by hydraulic collisions and shear forces within the FBC reactor. Table 3 presents an elemental analysis of FBC pellets following acid-digestion. The major impurities were Al (<1 wt%), attributable to the co-precipitation of aluminum in Al-etching in the LCD process, and Na and Si, which were formed because of the adjustment of pH using NaOH and the seed material, respectively. Approximately 82 wt% vivianite and 10 wt% silica sand were obtained. The water content of the crystal was below 5%, which is significantly less than that of the sludge that was formed by chemical precipitation.

Table 4 summarizes results concerning the precipitation of phosphate that were recently reported in the literature. Alkaline earth metal is a major precipitant that is utilized in the removal of phosphorus from aqueous solution. The recovery of struvite ($NH_4MgPO_4 \cdot 6H_2O$) is widely conducted using Mg^{2+} and NH_4^+ salts because struvite is an effective alternative rock phosphate fertilizer that is used in agriculture.[43,44] However, the formation of struvite requires the proper molar ratio of the ternary compound, and so may yield secondary compounds ($Mg_3(PO_4)_2 \cdot 22H_2O$ or $(Mg)_3(PO_4)_2 \cdot 8H_2O$).[45,46] Recovered hydroxylapatite (HAP) and dicalcium phosphate dehydrate (DCPD) may be sources of dental phosphate cement (FAp, $Ca_{10}(PO_4)_6F_2$), but the use of phosphate from wastewater is practically unacceptable to human bone and teeth enamel.[47] The authors previously evaluated the effectiveness of alkaline earth metals (Mg, Ca, Sr, Ba) in removing phosphate form synthetic wastewater using fluidized-bed homogeneous crystallization (FBHC);[48] they also have potential uses in conventional agriculture.[49] Given the cost-effectiveness, operational pH and removal efficiency that are associated with the use of phosphorus, rather than general salts, in the treatment of wastewater, the recycling of vivianite, or ferrous phosphate, is a highly feasible and economically favorable method of treatment, when the highly pure ferrous phosphate could be a potential source for manufacturing the Li-ion secondary battery.

4. Conclusions

The removal and recovery of phosphorus using an FBC reactor with silica sand as seeds were examined. Three operational

Table 4 Literature of phosphorus removal by recovery of various metal phosphates *via* precipitation and FBC

Precipitant	Ref.	Method	Products	Properties and efficiency
Mg, NH_4^+ (struvite)	17	Precipitation	$Mg_3(PO_4)_2 \cdot 22H_2O$, struvite	Assisted by electrochemistry (2 mA cm^{-2}), PR = 95.7%
	44	Precipitation	Bobierrite ($(Mg)_3(PO_4)_2 \cdot 8H_2O$), struvite	PR = 92% at [Mg]/[P] = 3, pH 9
	45	Precipitation	MMP ($MgKPO_4$), MSP ($MgNaPO_4$)	PR = 99%; *K* removal = 33%, at pH ranges of 8.5 to 11.5, [Mg]/[P] = 0.6 to 1.4
Ca	18	Precipitation	DCPD ($CaHPO_4$), Hap ($Ca_5(PO_4)_3(OH)$)	DCPD at pH 4.7–5.7; Hap at pH > 6.3
	19	Precipitation	Hap ($Ca_5(PO_4)_3(OH)$)	Use of calcite as seed, initial *P* = 10 ppm, PR = 94%
	46	Precipitation	Struvite and calcite using dolomite lime as precipitant	PR = 91%, initial *P* = 87 ppm, pH 8.0–8.5
	47	Integration of electrodialysis and crystallization	DCPD ($CaHPO_4$), Hap ($Ca_5(PO_4)_3(OH)$)	PR = 82.7%, initial *P* = 2.5 mM pH 11, [Ca]/[P] = 1.5
	48	FBC	Alkaline earth metal as precipitant to produce homogeneous $Me_5(PO_4)_3(OH)$	Initial *P* = 1000 ppm, for Mg, Ca, Ba, and Sr, PR = 78%, 99%, 97% and 99%, CR = 54%, 79%, 79% and 89% at pH 7.5, 6.5, 7.2 and 6.4, respectively
Ba	49	FBC	$BaHPO_4$, $Ba_3(PO_4)_2$	Barium removal = 98% at pH 8.4–8.8 and [Ba]/[P] = 1
Fe	This study	FBC	Vivianite ($Fe_3(PO_4)_2 \cdot 8H_2O$)	Real wastewater of TFT-LCD manufacturing, ~500 ppm-P; PR = 95%, CR = 60% at [Fe]/[P] = 1.5, pH 6

variables – pH, Fe/P molar ratio, and upflow velocity – were demonstrated to affect the efficiency of phosphate removal (PR) and the crystallization ratio (CR). Experimental results indicated that pH = 5.8 ± 0.2 maximized CR%. Increasing the upflow velocity increased the amount of crystal produced. The upflow velocity was maintained in the range 30.56–68.76 m h^{-1} (at a cross-section loading of 0.72 kg per P per h per m^2) to ensure sufficient collision between particles and promote the heterogeneous precipitation of ferrous phosphate. When the initial molar ratio of Fe/P was above 1.5 in treating the real wastewater containing *ca.* 500 ppm-P, the efficiencies of PR and CR were optimized to 95% and 63%, respectively. The SEM and XRD results verified that the recovery product was a pure vivianite phase in the form of pellets with an average size of 0.45 mm (from a seed of around 0.2 mm in diameter) following 200 h of FBC operation. Although the oxidation of Fe(II) could influence the purity of vivianite, as well as the future application in preparing $LiFePO_4$, the deep blue color of FBC pellets indicated that the amount of oxidized iron was insignificant. The recovery of vivianite crystals in this study highlighted the treatability of phosphorus wastewater using an FBC process.

Conflicts of interest

There are no conflicts to declare.

References

1 J. M. Abell, D. Özkundakci and D. P. Hamilton, *Ecosystems*, 2010, **13**, 966–977.
2 K. Meinikmann, M. Hupfer and J. Lewandowski, *J. Hydrol.*, 2015, **524**, 214–226.
3 R. W. Scholz, A. E. Ulrich, M. Eilitta and A. Roy, *Sci. Total Environ.*, 2013, **461–462**, 799–803.
4 S. H. Chuang, W. C. Chang, Y. H. Huang, C. C. Tseng and C. C. Tai, *Bioresour. Technol.*, 2011, **102**, 5461–5465.
5 B. L. Turner, A. W. Cheesman, L. M. Condron, K. Reitzel and A. E. Richardson, *Geoderma*, 2015, **257–258**, 1–3.
6 A. Ugurlu and B. Salman, *Environ. Int.*, 1988, **24**, 911–918.
7 T. C. Chen, Y. J. Shih, C. C. Chang and Y. H. Huang, *J. Taiwan Inst. Chem. Eng.*, 2013, **44**, 61–66.
8 C. C. Su, C. M. Chen, J. Anotai and M. C. Lu, *Chem. Eng. J.*, 2013, **222**, 128–135.
9 J. Zhao, D. Wang, X. Li, G. Zeng and Q. Yang, *RSC Adv.*, 2016, **6**, 86165–86173.
10 L. Ruihua, Z. Lin, T. Tao and L. Bo, *J. Hazard. Mater.*, 2011, **190**, 669–676.
11 J. Shi, D. Y. Yin, Z. W. Xu, D. M. Song and F. Cao, *RSC Adv.*, 2016, **6**, 68185–68192.
12 X. Zhang, H. J. Lin and B. Hu, *RSC Adv.*, 2016, **6**, 57960–57968.
13 A. Sendrowski and T. H. Boyer, *Desalination*, 2013, **322**, 104–112.
14 M. S. Rahaman, D. S. Mavinic, A. Meikleham and N. Ellis, *Water Res.*, 2014, **51**, 1–10.
15 P. Wilfert, P. S. Kumar, L. Korving, G. J. Witkamp and M. C. M. V. Loosdrecht, *Environ. Sci. Technol.*, 2015, **49**, 9400–9414.
16 Q. Ping, Y. Li, X. Wu, L. Yang and L. Wang, *J. Hazard. Mater.*, 2016, **310**, 261–269.
17 H. Huang, J. Liu, S. Wang, Y. Jiang, D. Xiao, L. Ding and F. Gao, *Ecol. Eng.*, 2016, **92**, 111–118.
18 L. Vasenko and H. Qu, *J. Cryst. Growth*, 2017, **459**, 61–66.
19 Y. Song, P. G. Weidler, U. Berg, R. Nüesch and D. Donnert, *Chemosphere*, 2006, **63**, 236–243.
20 E. Lacasa, P. Cañizares, C. Sáez, F. J. Fernández and M. A. Rodrigo, *Chem. Eng. J.*, 2011, **172**, 137–143.
21 S. Elabbas, N. Ouazzani, L. Mandi, F. Berrekhis, M. Perdicakis, S. Pontvianne, M. N. Pons, F. Lapicque and J. P. Leclerc, *J. Hazard. Mater.*, 2016, **319**, 69–77.
22 J. L. Campos, L. Otero, A. Franco, A. Mosquera-Corral and E. Roca, *Bioresour. Technol.*, 2009, **100**, 1069–1073.
23 M. M. Seckler, O. S. L. Bruinsma and G. M. Van Rosmalen, *Water Res.*, 1996, **30**, 1677–1685.
24 M. M. Seckler, M. L. J. van Leeuwen, O. S. L. Bruinsma and G. M. van Rosmalen, *Water Res.*, 1996, **30**, 1589–1596.
25 X. Ou, H. Gu, Y. Wu, J. Lu and Y. Zheng, *Electrochim. Acta*, 2013, **96**, 230–236.
26 Y. Liu, J. Gu, J. Zhang, J. Wang, N. Nie, Y. Fu, W. Li and F. Yu, *Electrochim. Acta*, 2015, **173**, 448–457.
27 F. C. Ballesteros, A. F. S. Salcedo, A. C. Vilando, Y. H. Huang and M. C. Lu, *Chemosphere*, 2016, **164**, 59–67.
28 M. M. Bello, A. A. A. Raman and M. Purushothaman, *J. Cleaner Prod.*, 2017, **141**, 1492–1514.
29 D. Villa-Gomez, H. Ababneh, S. Papirio, D. P. L. Rousseau and P. N. L. Lens, *J. Hazard. Mater.*, 2011, **192**, 200–207.
30 C. S. Chen, Y. J. Shih and Y. H. Huang, *Chem. Eng. J.*, 2015, **279**, 120–128.
31 Y. J. Shih, R. R. M. Abarca, M. D. G. de Luna, Y. H. Huang and M. C. Lu, *Chemosphere*, 2017, **173**, 466–473.
32 A. A. Borno and M. B. Tomson, *Geochim. Cosmochim. Acta*, 1994, **58**(24), 5373–5378.
33 L. Montastruc, C. Azzaro-Pantel, L. Pibouleau and S. Domenech, *Chem. Eng. Process.*, 2004, **43**, 1289–1298.
34 H. Takiyama, *Adv. Powder Technol.*, 2012, **23**, 273–278.
35 Y. Wang, K. H. Tng, H. Wu, G. Leslie and T. D. Waite, *Water Res.*, 2014, **57**, 140–150.
36 L. Pastor, D. Mangin, J. Ferrer and A. Seco, *Bioresour. Technol.*, 2010, **101**, 118–125.
37 C. C. Su, L. D. Dulfo, M. L. P. Dalida and M. C. Lu, *Sep. Purif. Technol.*, 2014, **125**, 90–96.
38 H. R. Diz and J. T. Novak, *J. Environ. Eng.*, 1998, **124**, 701–708.
39 C. Y. Tai, W. C. Chien and C. Y. Chen, *AIChE J.*, 1999, **45**, 1605–1614.
40 V. J. Inglezakis and S. G. Poulopoulos, *Adsorption, ion exchange and catalysis: design of operations and environmental applications*, Elsevier, Netherlands, 2006, ch. 3.
41 G. McGowan and J. Prangnell, *Geoarchaeology*, 2006, **21**, 93–111.

42 N. Sleiman, V. Deluchat, M. Wazne, M. Mallet, A. Courtin-Nomade, V. Kazpard and M. Baudu, *Colloids Surf., A*, 2017, **514**, 1–10.
43 H. Huang, P. Zhang, Z. Zhang, J. Liu, J. Xiao and F. Gao, *J. Cleaner Prod.*, 2016, **127**, 302–310.
44 Warmadewanthi and J. C. Liu, *Sep. Purif. Technol.*, 2009, **64**, 368–373.
45 K. Xu, J. Li, M. Zheng, C. Zhang, T. Xie and C. Wang, *Water Res.*, 2015, **80**, 71–79.
46 X. Liu, Z. Xu, J. Peng, Y. Song and X. Meng, *J. Environ. Sci.*, 2016, **44**, 260–268.
47 A. T. K. Tran, Y. Zhang, D. De Corte, J. B. Hannes, W. Ye, P. Mondal, N. Jullok, B. Meesschaert, L. Pinoy and B. Van der Bruggen, *J. Cleaner Prod.*, 2014, **77**, 140–151.
48 Y. J. Shih, H. C. Chang and Y. H. Huang, *J. Taiwan Inst. Chem. Eng.*, 2016, **62**, 177–186.
49 M. M. Rahman, M. A. M. Salleh, U. Rashid, A. Ahsan, M. M. Hossain and C. S. Ra, *Arabian J. Chem.*, 2014, **7**, 139–155.